

## **Multi-band Differential Photometry of the Eclipsing Variable Star NSVS 5750160**

**Robert C. Berrington**

*Ball State University, Dept. of Physics and Astronomy, Muncie, IN 47306; rberrington@bsu.edu*

**Erin M. Tuhey**

*Ball State University, Dept. of Physics and Astronomy, Muncie, IN 47306; emtuhey@bsu.edu*

*Received April 15, 2014; revised April 24, 2014; accepted April 25, 2014*

**Abstract** We present new multi-band differential aperture photometry of the eclipsing variable star NSVS 5750160. The light curves are analyzed with the Wilson-Devinney model to determine best-fit stellar models. Our models show that NSVS 5750160 is consistent with a W-type W Ursae Majoris eclipsing variable star, and require the presence of a spot to fit the observed O'Connell effect. Two different spot models are presented but neither model is conclusive.

### **1. Introduction**

The Northern Sky Variability Survey (NSVS; Woźniak *et al.* 2004) catalogue entry star 5750160 was originally classified as a W Ursae Majoris contact binary by Hoffman *et al.* (2009). The NSVS is a search for variability in the stars observed with the Robotic Optical Transient Search Experiment (ROSTE-I). The primary goal of the NSVS is to search for optical transients associated with quick response to Gamma-Ray Burst (GRB) events reported from satellites to measure optical light curves of GRB counterparts. When no GRB events were available ROSTE-I was devoted to a systematic sky patrol of the sky northward of declination  $-38^\circ$ . The star NSVS 5750160 can be found at the celestial coordinates R.A.  $20^{\text{h}}40^{\text{m}}52^{\text{s}}.4$ , Dec.  $+40^\circ 13' 18.6''$  (J2000.0). The automated classification system developed by Hoffman *et al.* (2009) reported a photometric period of  $P = 0.33847$  day.

In this paper we present a new extensive photometric study of this system. The paper is organized as follows. Observational data acquisition and reduction methods are presented in section 2. Time analysis of the photometric light curve and Wilson-Devinney models are presented in section 3. Discussion of the results and future directions are presented in section 4.

### **2. Observational data**

We present new three-filter photometry of the eclipsing variable star candidate NSVS 5750160. The data were taken by the Meade 0.4-meter Schmidt

Cassegrain telescope within the Ball State University observatory located atop the Cooper science complex. All exposures were acquired by a Santa Barbara Instruments Group (SBIG) STL-6303e camera through the Johnson-Cousins B, V, and R ( $R_c$ ) filters on the nights of July 24, 25, and 27, 2013. All images were bias- and dark-current subtracted, and flat-field corrected using the CCDRED reduction package found in the Image Reduction and Analysis Facility (IRAF; National Optical Astronomy Observatories 2014). All photometry presented in this study is differential aperture photometry, and was performed on the target eclipsing candidate and two comparison standards by the AIP4WIN photometry package (Berry and Burnell 2005). Over the three nights, a total of 406 images were taken in B and V, and 402 images in  $R_c$ . Figure 1 shows a representative exposure with the eclipsing star candidate and the two comparison stars marked. We have chosen the Tycho catalogue star (Hog *et al.* 1998) TYC 3170-822-1 as the primary comparison star (C1). The folded light curves (see section 3.1) for the instrumental differential B, V, and  $R_c$  magnitudes are shown in Figure 2. We define the differential magnitude by the variable star magnitude minus C1 (Variable–C1). Also shown in Figure 2 (bottom panel) is the differential V magnitude of C1 minus the second comparison star (C2) or the check star. The comparison light curve was inspected for variability. None was found.

Measured instrumental B and V differential magnitudes were reduced to Johnson B and V magnitudes by comparison with known calibrated magnitudes for C1. The star C1 has measured Johnson B and V magnitudes of  $11.44 \pm 0.06$  and  $10.71 \pm 0.05$ , respectively (Hog *et al.* 1998). The calibrated V light curve with the B–V color index versus orbital phase is shown in Figure 3 with error bars removed for clarity. Simultaneous B and V magnitudes are used to determine B–V colors by linear interpolating between measured B magnitudes to a similar time for measured V magnitudes.

### 3. Analysis

#### 3.1. Period analysis and ephemerides

Heliocentric Julian dates (HJD) for the observed times of minimum were calculated for each of the B, V, and R band light curves shown in Figure 2 for all observed primary and secondary minima. A total of two primary eclipses and four secondary eclipses were observed for each band. The times of minimum were determined by the algorithm described by Kwee and van Woerden (1956). Similar times of minimum from differing band passes were compared and no significant offsets or wavelength-dependent trends were observed. Similar times of minimum from each of the band passes were averaged together and reported in Table 1 along with  $1\sigma$  error bars.

Light curves were inspected by the PERANSO software (Vanmunster 2011) to determine orbital periodicity by applying the analysis of variance (ANOVA)

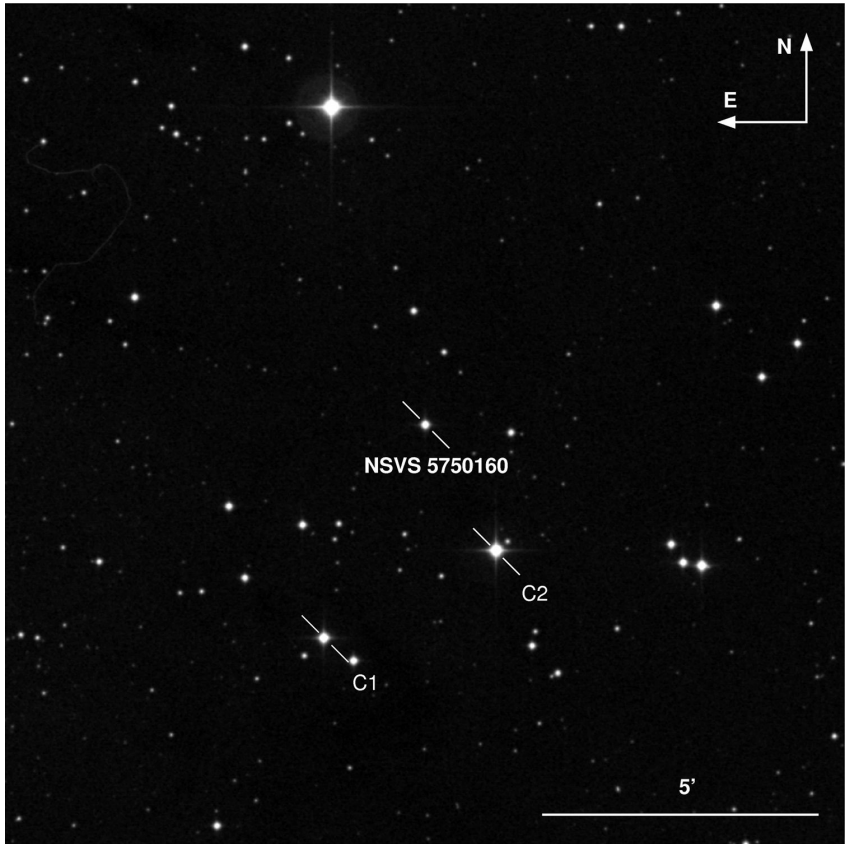


Figure 1. Star field containing the variable star NSVS 5750160. The location of the variable star is shown along with the comparison (C1) star and the check (C2) star used to calculate the differential magnitudes reported in Figure 2.

statistic which uses periodic orthogonal polynomials to fit observed light curves (Schwarzenberg-Czerny 1996). Our best-fit orbital period was found to be  $0.33847 \pm 0.00060$  day and is similar to the orbital period reported by Hoffman *et al.* (2009) which uses the photometric data reported by the NSV Survey (Woźniak *et al.* 2004). The resulting linear ephemeris becomes

$$T_{\min} = 2456492.85265(23) + 0.33847(60) E. \quad (1)$$

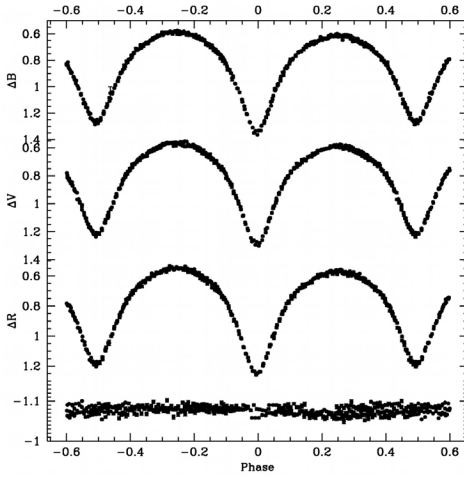


Figure 2. Folded light curves for differential aperture Johnson-Cousins B, V, and R magnitudes. Phase values are defined by Equation 2. Top three panels show the folded light curves for Johnson B (top panel), Johnson V (middle panel), and Cousins R (bottom panel) magnitudes. Bottom panel shows differential Johnson V band magnitudes for the comparison minus the check star. All error bars are  $1\sigma$  error bars with typical values  $<0.01$  magnitude (smaller than a point size). Repeated points do not show error bars (points outside the phase range of  $-0.5, 0.5$ ).

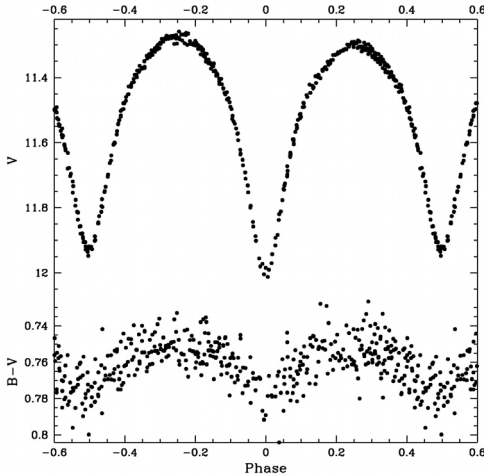


Figure 3. Folded light curve for differential aperture Johnson V magnitudes (top panel) and B-V color (bottom panel) versus orbital phase. Phase values are defined by Equation 2. Error bars are not shown for clarity. All B-V colors are calculated by subtracting linearly-interpolated B magnitudes from measured V magnitudes.

Table 1. Calculated heliocentric Julian dates (HJD) for the observed times of minimum of NSVS 5750160.

$T_{min}$	Eclipse	$E$	(O-C)
2456492.68280 $\pm$ 0.00022	s	-0.5	-0.000615
2456492.85265 $\pm$ 0.00023	p	0	0
2456493.69792 $\pm$ 0.00017	s	2.5	-0.000905
2456493.86810 $\pm$ 0.00021	p	3	0.00004
2456496.74478 $\pm$ 0.00029	s	11.5	-0.000275
2456497.76032 $\pm$ 0.00021	s	14.5	-0.000145

Notes: Observed times of minimum (column 1); the type of minimum (column 2). Observed minus Calculated (O-C) residual (column 4) values are given for the linear ephemeris given in Equation 1. Reported times are averaged from the individual B-, V-, and R-band times of minimum determined by the algorithm described by Kwee and van Woerden (1956). O-C values are given in units of days with primary eclipse values determined from integral epoch numbers, and secondary eclipse values determined from half integral epoch numbers (column 3).

Figure 2 shows the folded differential magnitudes versus orbital phase for NSVS 5750160 for the B, V, and R Johnson-Cousins bands folded over the period determined by the NSVS (see Equation 1). The orbital phase ( $\Phi$ ) is defined as:

$$\Phi = \frac{T - T_0}{P} - \text{Int} \left( \frac{T - T_0}{P} \right), \quad (2)$$

where  $T_0$  is the ephemeris epoch and is the time of minimum of a primary eclipse. Throughout this paper we will use the value of 2456492.68280 for  $T_0$ . The variable  $T$  is the time of observation, and  $P$  is the period of the orbit. The value of  $\Phi$  ranges from a minimum of 0 to a maximum of 1.0. All light curve Figures plot phase values (-0.6,0.6) where the negative values are given by  $\Phi - 1$ .

The Observed minus Calculated residual times of minimum (O-C) were determined from Equation 1 and are given in Table 1. The best-fit linear line determined by a linear regression to the O-C residual values is shown in Figure 4, and indicates the times of minima are well described by a period of 0.338511  $\pm$  0.000085 day, and is consistent with our previous determination of the orbital period at  $< 1\sigma$ .

Figure 5 shows the folded V band light curve measured from this study along with the measured values extracted from the NSV Survey (NSVS; Woźniak *et al.* 2004) with standard rejected flags set. The temporal coverage of the NSVS is sporadic and no individual times of minimum were observed over duration of the survey. Temporal coverage of NSVS spans one calendar year starting April 1, 1999 (JD 2451270) to March 30, 2000 (JD 2451633). All

magnitudes reported by NSVS are unfiltered CCD magnitudes whose range is limited by the sensitivity of the CCDs. Spectral response of CCD resulted in an effective wavelength best matched to the Johnson R band, but were calibrated to the Johnson V-band filter by comparison with Tycho catalogue stars and is the most likely explanation for the offset observed in Figure 5 between our measured V-band magnitudes and the NSVS V-band magnitudes. This indicates that both data sets are consistent with the ephemeris

$$T_{\text{min}} = 2456492.85265(23) + 0.338511(85) E, \quad (3)$$

and with the original period of 0.33847 day at  $<1\sigma$  deviation. Because of the sporadic coverage of NSVS, it is not possible to determine if the revised period reflects a possible period change or a more accurate period. As previously noted, when using only our photometric data, we derive a period of 0.33847 day, and it will be the assumed period for the remainder of this study unless otherwise noted.

Effective temperature and spectral type are estimated from the B–V color index values measured at orbital quadrature ( $\pm 0.25$  orbital phase) with a value of  $B-V = 0.75 \pm 0.07$ . This results in an estimated stellar mass  $M_{\star} = 0.98^{+0.05}_{-0.07} M_{\odot}$  derived from Equation 4 of Harmanec (1988). Effective temperatures and errors were estimated by Table 3 from Flower (1996) to be  $T_{\text{eff}} = 5413 \pm 200$  K. Interstellar extinction estimates following Schlafly and Finkbeiner (2011) at the galactic coordinates for the object are unreliable due to the object's proximity to the galactic plane. These interstellar extinction models are based on line-of-sight galactic column densities. Along with the clumpy nature of the dust distribution in the galactic plane, there are a number of points that indicate that the B–V value is near the correct value. The corresponding stellar spectral type for the observed B–V is G8 (Johnson 1966). The light curve shows evidence of a star spot, seen in later-type stars and consistent with the estimated spectral type (see section 3.3). Furthermore, we report consistent distance estimates to the object using two different techniques (see section 4). The observed B–V was used to estimate the effective temperature, and became the starting point for subsequent stellar modeling. To confirm these conclusions, spectroscopic follow-up to confirm the spectral type, interstellar reddening, and radial velocities to measure stellar masses is necessary to gain further insight.

### 3.2. Light curve analysis

All observations taken during this study were analyzed using the Physics of Eclipsing Binaries (PHOEBE) software package (Prša and Zwitter 2005). The PHOEBE software package is a modeling package that provides a convenient, intuitive graphical user interface (GUI) to the Wilson-Devinney (WD) code (Wilson and Devinney 1971). In the version of PHOEBE used in this study, several advancements have been included in the package that facilitate the fitting

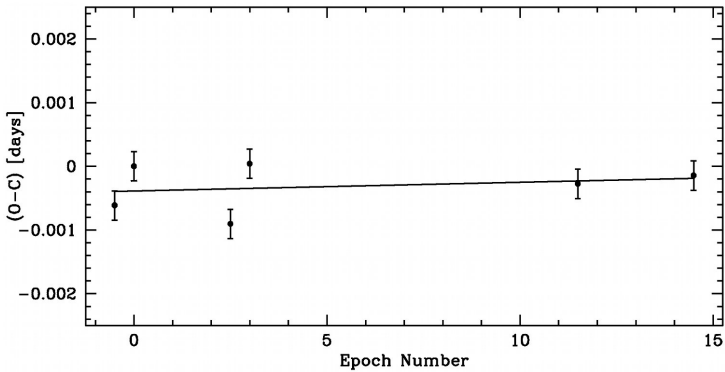


Figure 4. Observed minus calculated residual times of minimum (O-C) versus orbital epoch number. All point values are given in Table 1. Secondary times of minimum are plotted at half integer values, and all error bars are  $1\sigma$  error bars. Solid curve shows the best-fit linear line determined by a linear regression fit to the O-C residual values.

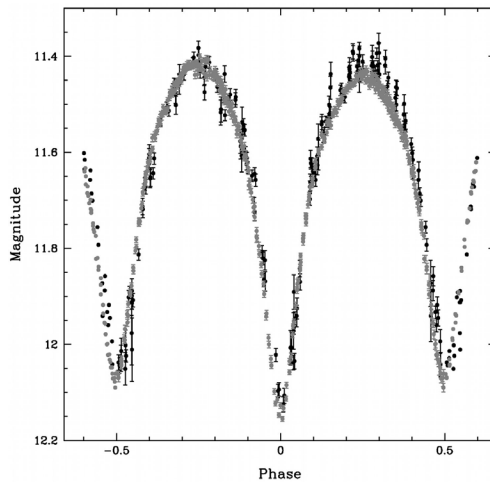


Figure 5. Folded light curve for Johnson V magnitudes. Gray points are measured magnitudes from the Ball State University 0.4m telescope. Measured values from the NSV Survey (Woźniak *et al.* 2004) are shown by the black points. All error bars are  $1\sigma$  error bars. Repeated points do not show error bars.

process. These include the inclusion of the Nedler and Mead downhill simplex (Nedler and Mead 1965) minimization algorithm into the fitting procedure that greatly increases the chance of a successful model convergence (Prša and Zwitter 2005).

All three Johnson-Cousins B, V, and  $R_c$  bands were fit simultaneously by the following procedure. Initial fits were performed assuming a common convective

envelope in direct thermal contact, resulting in a common surface temperature of  $T_{\text{eff}} = 5413 \text{ K}$  determined by the procedure discussed in section 3.1. Orbital period was set to the value of  $0.33847 \pm 0.00060$  day. Surface temperatures imply that the outer envelopes are convective, so the gravity brightening coefficients  $\beta_1$  and  $\beta_2$ , defined by the flux dependency  $F \propto g^\beta$ , were initially set at the common value consistent with a convective envelope of 0.32 (Lucy 1967). The more recent studies of Alencar and Vaz (1997) and Alencar *et al.* (1999) predict values for  $\beta \approx 0.4$ . These values were also used and had no effect on the resulting best-fit model. We adopted the standard stellar bolometric albedo  $A_1 = A_2 = 0.5$  as suggested by Ruciński (1969), with two possible reflections.

The fitting procedure was used to determine the best-fit stellar models and orbital parameters from the observed light curves shown in Figure 2. Initial fits were performed assuming a common convective envelope in thermal contact which assumes similar surface temperatures for both stars. After normalization of the stellar luminosity, the light curve was crudely fit by altering the stellar shape by fitting the Kopal ( $\Omega$ ) parameter. The Kopal parameter describes the equipotential surface that the stars fill. For overcontact binaries, this has the effect of determining the shape of the stars, and has a strong effect on the global morphology of the light curve.

Initial fits were performed assuming the outer convective envelope was in thermal contact, and therefore both the primary and secondary stars have similar effective temperatures ( $T_{\text{eff}}$ ). After the fit could no longer be improved, we started to consider the other parameters to fit the light curve. These parameters included the effective temperature of the primary star  $T_{\text{eff},1}$ , the mass ratio  $q = M_2/M_1$ , and the orbital inclination  $i$ . It became apparent that the models could not represent the observed light curve without decoupling stellar luminosities from  $T_{\text{eff}}$ . We interpreted this as evidence that the stars were not in thermal contact and therefore could have differing surface temperatures. All further model fits were performed assuming the primary and secondary components were not in thermal contact.

All model fits were performed with a limb darkening correction. The limb-darkening correction takes the form

$$\mathcal{L}_\lambda(\mu) = 1 - x_\lambda(1 + \mu) - y_\lambda f_\lambda(\mu) \quad (4)$$

where  $\mu = \cos(\varphi)$  and represents the cosine of the angle ( $\varphi$ ) with the emergent luminosity normal to the stellar surface. The function  $\mathcal{L}_\lambda(\mu)$  is the ratio of the emergent luminosity at a given  $\mu$  with the emergent luminosity normal ( $\mu = 1$ ) to the stellar surface. The coefficients  $x_\lambda$  and  $y_\lambda$  are determined by stellar properties and are known as the linear and non-linear coefficients, respectively. Finally, the function  $f_\lambda(\mu)$  is the non-linear functional form of the limb-darkening correction. PHOEBE allows for differing functional forms to be specified by the user for the non-linear component. Studies by Diaz-Cordoves and Gimenez



(1992) and van Hamme (1993) have shown that early type stars ( $T_{\text{eff}} > 9000\text{K}$ ) are best fit by a square root law given by the functional form ( $f_{\lambda}(\mu) = (1 - \sqrt{\mu})$ ). Late type stars ( $T_{\text{eff}} < 9000\text{K}$ ) are best described by the logarithmic law first suggested by Klinglesmith and Sobieski (1970) and given by the functional form ( $f_{\lambda}(\mu) = \mu \log(\mu)$ ). In our study, fits were attempted for both laws. In both cases, the values for the linear ( $x_{\lambda}$ ) and non-linear ( $y_{\lambda}$ ) coefficients were determined at each fitting iteration by the van Hamme (1993) interpolation Tables. In both cases our best-fit models used the logarithmic law, and therefore support the conclusions of Diaz-Cordoves and Gimenez (1992) and van Hamme (1993).

Figures 6–8 show the folded Johnson B-, Johnson V-, and Cousins R-band light curves along with the synthetic light curve calculated by the best-fit model, respectively. The best-fit models were determined by the aforementioned fitting procedure. Note how the synthetic light curve consistently under-predicts the observed light curve for phases in the interval  $-0.5, 0$ , and over-predicts for phases in the interval  $0, 0.5$ . The parameters, along with  $1\sigma$  error bars describing this best-fit model, are given in column 2 of Table 2. The best-fit model is consistent with an overcontact binary described by a filling factor  $\mathcal{F} = 0.0677$ . The filling factor is defined by the inner and outer critical equipotential surfaces that pass through the  $L_1$  and  $L_2$  Lagrangian points of the system. For our system the these equipotential surfaces are  $\Omega(L_1) = 4.265$  and  $\Omega(L_2) = 3.697$ .

### 3.3 Spot model

It is apparent from Figures 6–8 that the previous model is unable to reproduce accurately the observed light curve. To improve the fit, a single spot was necessary. Unfortunately, all we have at our disposal are the observed light curves, and differing spot models may be degenerate to the observed light curve.

Initial models started from the model without spots determined in section 3.2. We were unsuccessful with simultaneous convergence of the remaining parameters. Both the spot radius and spot longitude also eluded successful convergence. All fits were performed by manually changing the spot radius, then converging the spot temperature factor. Once a satisfactory convergence was determined, the spot parameters were then held fixed and the stellar parameters were then allowed to converge to the final model. Figures 9–11 show the final best-fit stellar model.

The best-fit model with a single cool spot on the primary star is given in Table 3. Spot parameters given by the WD model are the longitude  $\theta$ , colatitude  $\phi$ , radius  $\rho$ , and temperature factor ( $\tau = T_{\text{spot}} / T_{\text{eff}}$ ). The spot longitude is measured counterclockwise (CCW) relative to orbital motion from the  $L_1$  Lagrangian point. Spot colatitude is measured from stellar rotation axis with the equator represented by  $\phi = 90^\circ$ . Light curves were found to be minimally dependent on the spot's colatitude and therefore difficult to converge when allowed to vary. All spot models restricted spots to be located on the equator ( $\phi = 90^\circ$ ).

Table 2. Model parameters determined by the best-fit WD model as fit in sections 3.2 and 3.3.

Parameter	Symbol <sup>1</sup>	Best fit (spots not allowed)	Value	Best fit (spots allowed)
Period	P [days]	$0.338511 \pm 0.000085$		$0.338511 \pm 0.000085$
Epoch	$T_0$ [HJD]	$2456492.85265 \pm 0.00023$		$2456492.85265 \pm 0.00023$
Inclination	$i$ [°]	$79.35 \pm 0.05$		$79.05 \pm 0.04$
Surface Temperature <sup>2</sup>	$T_{\text{eff},1}$ [K]	$5290 \pm 200$		$5253 \pm 200$
Surface Temperature <sup>2</sup>	$T_{\text{eff},2}$ [K]	$5167 \pm 200$		$5133 \pm 200$
Surface Potential <sup>3</sup>	$\Omega_{1,2}$ [—]	$4.227 \pm 0.002$		$4.081 \pm 0.002$
Limb Darkening	$x_{\text{bol},1,2}$	0.608		0.607
Limb Darkening	$y_{\text{bol},1,2}$	0.167		0.180
Limb Darkening	$x_{\text{B},1,2}$	0.754		0.754
Limb Darkening	$y_{\text{B},1,2}$	-0.144		-0.128
Limb Darkening	$x_{\text{V},1,2}$	0.739		0.740
Limb Darkening	$y_{\text{V},1,2}$	0.099		0.115
Limb Darkening	$x_{\text{R},1,2}$	0.677		0.680
Limb Darkening	$y_{\text{R},1,2}$	0.219		0.232

<sup>1</sup> 1 for primary stellar component, 2 for secondary stellar component. <sup>2</sup> Errors estimated from color values in Figure 3. <sup>3</sup> Surface potential for both stars (contact/overcontact binaries) defined to be equal for both stars. Note: Errors 1 $\sigma$  except where otherwise given.

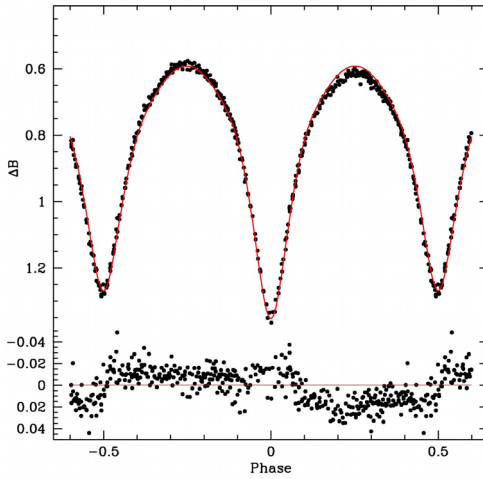


Figure 6. Best-fit WD model fit without spots (solid curve) to the folded light curve for differential aperture Johnson B (top panel). The best-fit orbital parameters used to determine the light curve model are given in Table 2. The bottom curve shows residuals from the best-fit model (solid curve). Error bars are omitted from the points for clarity.

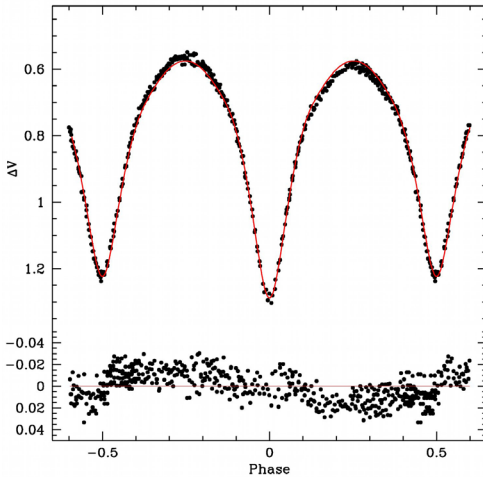


Figure 7. Best-fit WD model fit without spots (solid curve) to the folded light curve for differential aperture Johnson V (top panel). The best-fit orbital parameters used to determine the light curve model are given in Table 2. The bottom curve shows residuals from the best-fit model (solid curve). Error bars are omitted from the points for clarity.

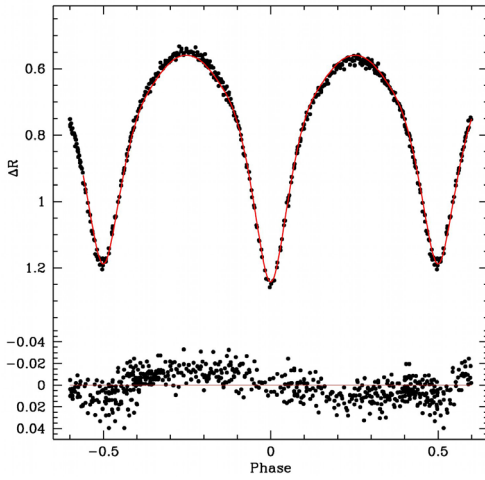


Figure 8. Best-fit WD model fit without spots (solid curve) to the folded light curve for differential aperture Cousins R (top panel). The best-fit orbital parameters used to determine the light curve model are given in Table 2. The bottom curve shows residuals from the best-fit model (solid curve). Error bars are omitted from the points for clarity.

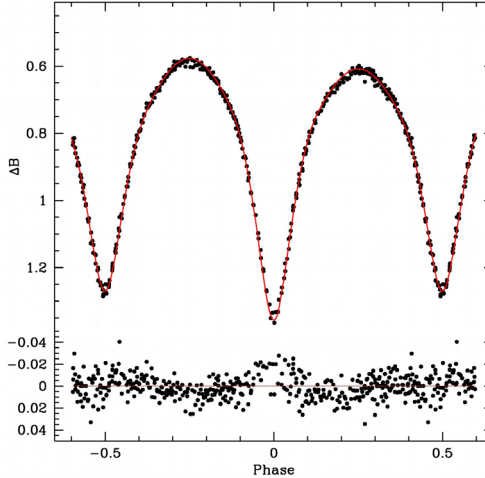


Figure 9. Best-fit WD model fit with spots (solid curve) to the folded light curve for differential aperture Johnson B (top panel). The best-fit orbital parameters used to determine the light curve model are given in Table 2. The bottom panel shows residuals from the best-fit model (solid curve). Error bars are omitted from the points for clarity.

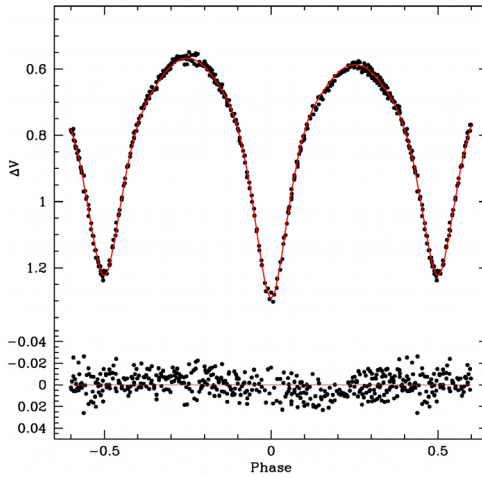


Figure 10. Best-fit WD model fit with spots (solid curve) to the folded light curve for differential aperture Johnson V (top panel). The best-fit orbital parameters used to determine the light curve model are given in Table 2. The bottom panel shows residuals from the best-fit model (solid curve). Error bars are omitted from the points for clarity.

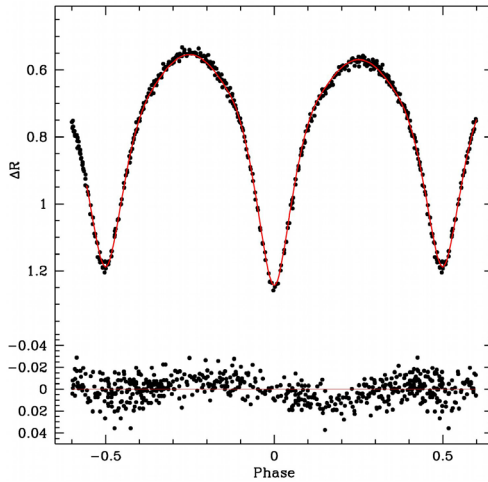


Figure 11. Best-fit WD model fit with spots (solid curve) to the folded light curve for differential aperture Cousins R (top panel). The best-fit orbital parameters used to determine the light curve model are given in Table 2. The bottom panel shows residuals from the best-fit model (solid curve). Error bars are omitted from the points for clarity.

Table 3. Best-fit Spot models. All parameters are for the primary stellar component.

<i>Description</i>	<i>Parameter</i>	<i>Cold Spot Model</i>	<i>Hot Spot Model</i>
Spot colatitude	$\phi_1 [^\circ]$	90	90
Spot longitude	$\lambda_1 [^\circ]$	270	90
Spot radius	$\rho_1 [^\circ]$	11	13
Temperature	$\tau_1$	0.77	1.11

Table 4. Absolute parameters used to determine best-fit models.

<i>Parameter</i>	<i>Value</i>
$M_1 [M_\odot]$	0.84
$M_2 [M_\odot]$	1.12
$a [R_\odot]$	2.56
$R_1 [R_\odot]$	0.92
$R_2 [R_\odot]$	1.05
$\log(g_1) [\text{cm s}^{-2}]$	4.43
$\log(g_2) [\text{cm s}^{-2}]$	4.44
$\bar{\rho}_1 [\text{g cm}^{-3}]$	1.51
$\bar{\rho}_2 [\text{g cm}^{-3}]$	1.40
$M_{\text{bol},1}$	5.34
$M_{\text{bol},2}$	5.16

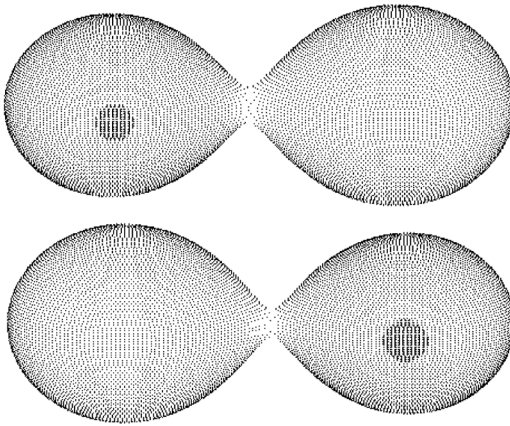


Figure 12. Graphical representation for the best-fit cold spot WD model (top panel) and hot spot WD model (bottom panel). The best-fit orbital parameters used to determine the light curve model are given in Table 2.

In our second attempt we tried a single hot spot on the primary but on the opposite side of the star. Best fits were determined using the algorithm described above. Spot parameters are given in Table 3. Fits were similar to the cool spot model fits with similar residuals to those for the cold spot model. Graphical representations for both the hot spot WD model and the cold spot WD model are shown in Figure 12.

#### 4. Discussion and conclusions

Figure 5 shows a comparison of the NSVS light curve with the light curve measured during this study. It is immediately apparent that the NSVS light curve shows similar heights for max I ( $\Phi = 0.25$ ) and max II ( $\Phi = -0.25$ ). Differing heights between max I and max II is known as the O'Connell (1951) effect. In contrast the light curve measured during this study does show a positive (max I > max II) O'Connell effect. Numerous models have been presented as a possible explanation, but many deal with impacting (Shaw 1994) or absorbing (O'Connell 1951) gas streams which are unlikely for overcontact binaries. As we showed in section 3.3, a model with a single spot can explain the observed O'Connell effect.

Given the absolute parameters in Table 4, we can estimate the distance to NSVS 5750160. Taken from Flower (1996), the bolometric corrections (BC) used for the primary and secondary star are  $BC_1 = -0.195$  and  $BC_2 = -0.237$ , respectively. From the bolometric magnitudes reported in Table 4 and the BC, the combined visual magnitude is  $M_V = 4.28$ . Furthermore, Ruciński and Duerbeck (1997) determined that the absolute visual magnitude is given by

$$M_V = -4.44 \log_{10}(P) + 3.02(B - V) + 0.12 \quad (5)$$

to within an accuracy of  $\pm 0.1$ . Our calculated value differs from the absolute magnitude determined from Equation 5 ( $M_V = 4.47$ ) by 0.19 magnitude. This agreement ( $< 2\sigma$ ) in the absolute visual magnitudes confirms the initial determination of  $M_V$ . The distance modulus of the system ( $m - M$ ) = 6.97 for our calculated value, and 6.78 for value obtained from Equation 5. This corresponds to a distance of 247.8 pc and 227.8 pc, respectively. Agreement of these distance estimates also supports our conclusions regarding the interstellar extinction from section 3.1.

Stellar mean densities ( $\bar{\rho}$ ) are given in Table 4, and Mochnacki (1981) showed they are given by

$$\bar{\rho}_1 = \frac{0.0189}{r_1^3(1+q)P^2}, \quad \bar{\rho}_2 = \frac{0.0189q}{r_2^3(1+q)P^2}, \quad (6)$$

where the stellar radius  $r$  is normalized to the semimajor axis. We determined

the values for the primary and secondary components to be  $1.51 \text{ g cm}^{-3}$  and  $1.40 \text{ g cm}^{-3}$ , respectively.

This study has confirmed that NSVS 5750160 is a W UMa contact binary not in thermal contact, and with the hotter, smaller star eclipsed during primary minimum it is a member of the W-type subclass. Our measured light curve shows a positive O'Connell (1951) effect which could not be explained without the presence of stellar spots. We showed that light curve can be well described by the presence of either a cool or a warm star spot on the primary star. However, we cannot exclude possible alternative explanations, and comment that further spectroscopic studies will greatly enhance our knowledge of this system.

## References

- Alencar, S. H. P., and Vaz, L. P. R. 1997, *Astron. Astrophys.*, **326**, 257.
- Alencar, S. H. P., Vaz, L. P. R., and Nordlund, Å. 1999, *Astron. Astrophys.*, **346**, 556.
- Berry, R., and Burnell, J. 2005, AIP4WIN (version 2.2.0), provided with *The Handbook of Astronomical Image Processing*, Willmann-Bell, Richmond, VA.
- Diaz-Cordoves, J., and Gimenez, A. 1992, *Astron. Astrophys.*, **259**, 227.
- Flower, P. J. 1996, *Astrophys. J.*, **469**, 355.
- Harmanec, P. 1988, *Bull. Astron. Inst. Czechoslovakia*, **39**, 329.
- Hoffman, D. I., Harrison, T. E., and McNamara, B. J. 2009, *Astron. J.*, **138**, 466.
- Hog, E., Kuzmin, A., Bastian, U., Fabricius, C., Kuimov, K., Lindegren, L., Makarov, V. V., and Roeser, S. 1998, *Astron. Astrophys.*, **335**, L65.
- Johnson, H. L. 1966, *Ann. Rev. Astron. Astrophys.*, **4**, 193.
- Klinglesmith, D. A., and Sobieski, S. 1970, *Astron. J.*, **75**, 175.
- Kwee, K. K., and van Woerden, H. 1956, *Bull. Astron. Inst. Netherlands*, **12**, 327.
- Lucy, L. B. 1967, *Z. Astrophys.*, **65**, 89.
- Mochnecki, S. W. 1981, *Astrophys. J.*, **245**, 650.
- National Optical Astronomy Observatories. 2014, CCDRED, reduction package in the Image Reduction and Analysis Facility (IRAF; <http://iraf.net/>), version 2.16.
- Nedler, J. A., and Mead, R. 1965, *Comput. J.*, **7**, 308.
- O'Connell, D. J. K. 1951, *Publ. Riverview College Obs.*, **2**, 85.
- Prša, A., and Zwitter, T. 2005, *Astrophys. J.*, **628**, 426 (PHOEBE software package v0.31a).
- Ruciński, S. M. 1969, *Acta Astron.*, **19**, 245.
- Ruciński, S. M., and Duerbeck, H. W. 1997, *Publ. Astron. Soc. Pacific*, **109**, 1340.
- Schlafly, E. F., and Finkbeiner, D. P. 2011, *Astrophys. J.*, **737**, 103.
- Schwarzenberg-Czerny, A. 1996, *Astrophys. J., Lett. Ed.*, **460**, L107.
- Shaw, J. S. 1994, *Mem. Soc. Astron. Ital.*, **65**, 95.



van Hamme, W. 1993, *Astron. J.*, **106**, 2096.

Vanmunster, T. 2011, Light Curve and Period Analysis Software, PERANSO v.2.50  
(<http://www.cbabelgium.com>).

Wilson, R. E., and Devinney, E. J. 1971, *Astrophys. J.*, **166**, 605.

Woźniak, P. R., *et al.* 2004, *Astron. J.*, **127**, 2436.